



AFRL-RX-WP-TR-2017-0416

REALIZATION OF CONFIGURABLE ONE-DIMENSIONAL REFLECTARRAY

Tony Low, and Sang-Hyun Oh

Regents Of The University Of Minnesota

Joseph Tischler

Naval Research Lab (NRL)

31 AUGUST 2017

Final Report

**Distribution Statement A.
Approved for public release; distribution is unlimited.**

**AIR FORCE RESEARCH LABORATORY
MATERIALS AND MANUFACTURING DIRECTORATE
WRIGHT-PATTERSON AIR FORCE BASE, OH 45433-7750
AIR FORCE MATERIEL COMMAND
UNITED STATES AIR FORCE**

NOTICE AND SIGNATURE PAGE

Using Government drawings, specifications, or other data included in this document for any purpose other than Government procurement does not in any way obligate the U.S. Government. The fact that the Government formulated or supplied the drawings, specifications, or other data does not license the holder or any other person or corporation; or convey any rights or permission to manufacture, use, or sell any patented invention that may relate to them.

This report is the result of contracted fundamental research deemed exempt from public affairs security and policy review in accordance with SAF/AQR memorandum dated 10 Dec 08 and AFRL/CA policy clarification memorandum dated 16 Jan 09. This report is available to the general public, including foreign nationals.

Copies may be obtained from the Defense Technical Information Center (DTIC)
(<http://www.dtic.mil>).

AFRL-RX-WP-TR-2017-0416 HAS BEEN REVIEWED AND IS APPROVED FOR
PUBLICATION IN ACCORDANCE WITH ASSIGNED DISTRIBUTION STATEMENT.

 //SIGNATURE//
SHIN MOU
Project Engineer
Nanoelectronic Materials Branch
Functional Materials Division
Materials and Manufacturing Directorate

 //SIGNATURE//
MARK G. SCHMITT
Branch Chief
Nanoelectronic Materials Branch
Functional Materials Division
Materials and Manufacturing Directorate

This report is published in the interest of scientific and technical information exchange, and its publication does not constitute the Government's approval or disapproval of its ideas or findings.

REPORT DOCUMENTATION PAGE

Form Approved
OMB No. 0704-0188

The public reporting burden for this collection of information is estimated to average 1 hour per response, including the time for reviewing instructions, searching existing data sources, gathering and maintaining the data needed, and completing and reviewing the collection of information. Send comments regarding this burden estimate or any other aspect of this collection of information, including suggestions for reducing this burden, to Department of Defense, Washington Headquarters Services, Directorate for Information Operations and Reports (0704-0188), 1215 Jefferson Davis Highway, Suite 1204, Arlington, VA 22202-4302. Respondents should be aware that notwithstanding any other provision of law, no person shall be subject to any penalty for failing to comply with a collection of information if it does not display a currently valid OMB control number. **PLEASE DO NOT RETURN YOUR FORM TO THE ABOVE ADDRESS.**

1. REPORT DATE (DD-MM-YY) 15 July 2017		2. REPORT TYPE Final		3. DATES COVERED (From - To) 15 June 2016 – 15 June 2017	
4. TITLE AND SUBTITLE Realization of Configurable One-Dimensional Reflectarray				5a. CONTRACT NUMBER FA8650-16-2-7640	
				5b. GRANT NUMBER	
				5c. PROGRAM ELEMENT NUMBER 65502E	
6. AUTHOR(S) Tony Low, and Sang-Hyun Oh - Regents Of The University Of Minnesota Joseph Tischler - Naval Research Lab (NRL)				5d. PROJECT NUMBER DARPA	
				5e. TASK NUMBER	
				5f. WORK UNIT NUMBER X17E	
7. PERFORMING ORGANIZATION NAME(S) AND ADDRESS(ES) University Of Minnesota 200 Union St. S.E. Minneapolis MN 55455-200				8. PERFORMING ORGANIZATION REPORT NUMBER U.S. Naval Research Laboratory 4555 Overlook Avenue SW Washington DC	
9. SPONSORING/MONITORING AGENCY NAME(S) AND ADDRESS(ES) Air Force Research Laboratory Materials and Manufacturing Directorate Wright-Patterson Air Force Base, OH 45433 Air Force Materiel Command United States Air Force				10. SPONSORING/MONITORING AGENCY ACRONYM(S) AFRL/RXAN	
				11. SPONSORING/MONITORING AGENCY REPORT NUMBER(S) AFRL-RX-WP-TR-2017-0416	
12. DISTRIBUTION/AVAILABILITY STATEMENT Distribution Statement A. Approved for public release; distribution is unlimited.					
13. SUPPLEMENTARY NOTES Report contains color.					
14. ABSTRACT (Maximum 200 words) A fundamental challenge remains in dynamically controlling the steering of long wavelength radiation ($\lambda > 8 \mu\text{m}$) using metal nanostructures or metamaterials (with critical dimensions $\sim 10 \text{ nm}$), where one is faced with a large scale mismatch up to 4-5 orders of magnitude and therefore intrinsically weak light-matter interactions. Here we report the proof-of-principle demonstration of anomalous reflection, where simulations and experiments show strong signatures of beam steering that are dependent upon graphene doping. This seed grant has allowed our team to establish the essential operating procedures (i.e. modeling, fabrication, and scatterometry) for the eventual realization of efficient, electrically-configurable, graphene-based, one-dimensional reflectarrays. Several immediate improvements to the device design and process flow are essential to suppress specular components of the reflected beams.					
15. SUBJECT TERMS DAPRA report, graphene, reflectarray, beamforming, anomalous reflection, plasmons, steering, dynamic, nanoribbons					
16. SECURITY CLASSIFICATION OF:			17. LIMITATION OF ABSTRACT: SAR	18. NUMBER OF PAGES 20	19a. NAME OF RESPONSIBLE PERSON (Monitor) Shin Mou
a. REPORT Unclassified	b. ABSTRACT Unclassified	c. THIS PAGE Unclassified			

Table of Contents

<u>Section</u>	<u>Page</u>
List of Figures	ii
Summary	1
Fabrication and packaging of GNR reflect-array.....	2
Modeling of GNR reflectarray.....	4
Scatterometry measurement.....	7
Exploring braoder device applications.....	11
Future Plans	13
References.....	14
LIST OF SYMBOLS, ABBREVIATIONS, AND ACRONYMS	15

List of Figures

<u>Figure</u>	<u>Page</u>
Figure 1. Proposed device platform for achieving tunable anomalous reflection of mid-IR light.	1
Figure 2. Fabrication schematics of graded graphene nano-ribbon reflectarray with lossless air-spacers.	2
Figure 3. Images of a GNR reflectarray. (a) Photograph of a GNR reflectarray chip. (b) Zoomed-in image of GNR reflectarray with alignment marks. The size of GNR patterns is 200 μm by 200 μm . (c) CAD image of GNR pattern including five supercells.	3
Figure 4. SEM images of a supercell of GNR reflectarray on CaF ₂ . The horizontal length of a supercell including 200 GNRs is 40 μm	3
Figure 5. Reflected field off the graphene reflectarray device for (a) normal and (b) oblique (10 degrees off normal) incident light.	4
Figure 6. Normalized far-field intensity as function of angle for different dopings for normal incident light. Specular beams are at zero degrees.	5
Figure 7. (a) Impact of dielectric loss on scattering phase. (b) Complex plane plot of the reflection coefficient for analytical model of the structure as a single port resonator.	6
Figure 8. Schematic of the scatterometer setup.	7
Figure 9. Schematic of the doping configuration.	8
Figure 10. (a) Fractional polarized reflectance of uniform GNR pattern with width of 150 nm, where light is polarized parallel (red) and perpendicular to the GNRs. (b) Extinction spectra for GNR pattern of varying ribbons width.	9
Figure 11. Normalized scattering intensity as a function of detector angle, and relative intensity of scattering peaks normalized to intensity of peak 1.	10
Figure 12. Schematics showing how one can utilize the graphene based reflectarray for various functionalities such as (b) cloaking, (c) illusion, (d) anomalous reflection, and (e) focusing.	11
Figure 13. Simulation results for reflective focusing off arbitrary surface.	12

Summary

A fundamental challenge remains in dynamically controlling the steering of long wavelength radiation ($\lambda > 8 \mu\text{m}$) using metal nanostructures or metamaterials (with critical dimensions ~ 10 nm), where one is faced with a large scale mismatch up to 4-5 orders of magnitude and therefore intrinsically weak light-matter interactions. Here we report the proof-of-principle demonstration of anomalous reflection, where simulations and experiments show strong signatures of beam steering that are dependent upon graphene doping. This seed grant has allowed our team to establish the essential operating procedures (i.e. modeling, fabrication, and scatterometry) for the eventual realization of efficient, electrically-configurable, graphene-based, one-dimensional reflectarrays. Several immediate improvements to the device design and process flow are essential to suppress specular components of the reflected beams. We believe our team is well-positioned to demonstrate dynamic tuning of anomalous beam in the next phase, if funding for this program is to be continued.

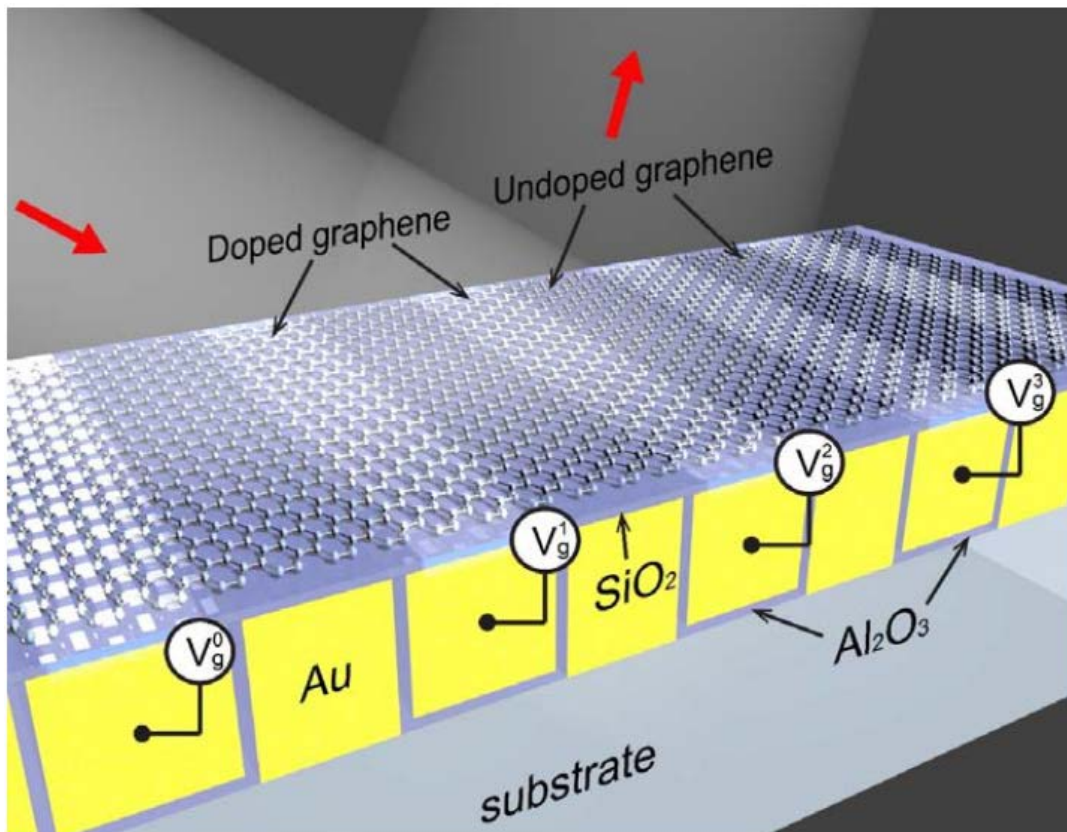


Figure 1. Proposed device platform for achieving tunable anomalous reflection of mid-IR light.

While the high carrier concentration in metals prohibit dynamic tuning of light-matter interactions, graphene can provide unique capabilities to help dynamically tune the reflection and transmission amplitude and direction of light. Fabrication and packaging of GNR reflect-array

Fabrication and packaging of GNR reflect-array

Graphene nano-ribbon (GNR) reflectarrays that allow for the control of anomalous reflection were designed by integrating a backside Au mirror to enhance the coupling efficiency of incident IR light. Such structures that integrate a dielectric spacer and backside mirror have been explored by many research groups. However, alumina (Al_2O_3) or silica (SiO_2), which often serves as a spacer, has an intrinsic absorption in IR regime for wavelengths greater than $8\ \mu\text{m}$. As such, it is impossible to obtain the full phase change needed to control anomalous reflection from graded GNR reflectarrays in this spectral range. In this project, we have solved this problem by developing GNR reflectarrays on a lossless air-spacer, as illustrated in Figure 2. This is achieved by 1) transferring graphene onto a CaF_2 substrate using a wet transfer method, 2) patterning the transferred graphene into graded GNRs with different widths using PMMA and electron-beam lithography, 3) the Au mirror with air-spacer is then combined with the CaF_2 substrate with graded GNRs, as shown in Figure 2c. The $2\text{-}\mu\text{m}$ -sized silica bead powders were mixed with optical epoxy (NOA 61) and a mixture of silica beads and optical epoxy was applied to four corners of the Au mirror substrate, followed by inverting the CaF_2 substrate with graded GNRs onto silica beads, thus creating an air-gap whose thickness is defined by the bead size. The uniformity of the air-spacer was confirmed by measuring the interference image generated from the air-gap. The air-spacer created by silica beads is open to the outside, making it possible to dope GNR chemically with nitric acid vapor. In addition to the chemical doping, a Au mirror substrate can work as a back-gate for electrical doping of a GNR. In the first year, thus far we employed a chemical doping approach. However, our goal for the future is to incorporate a back-gate for electrical doping using a Au mirror substrate.

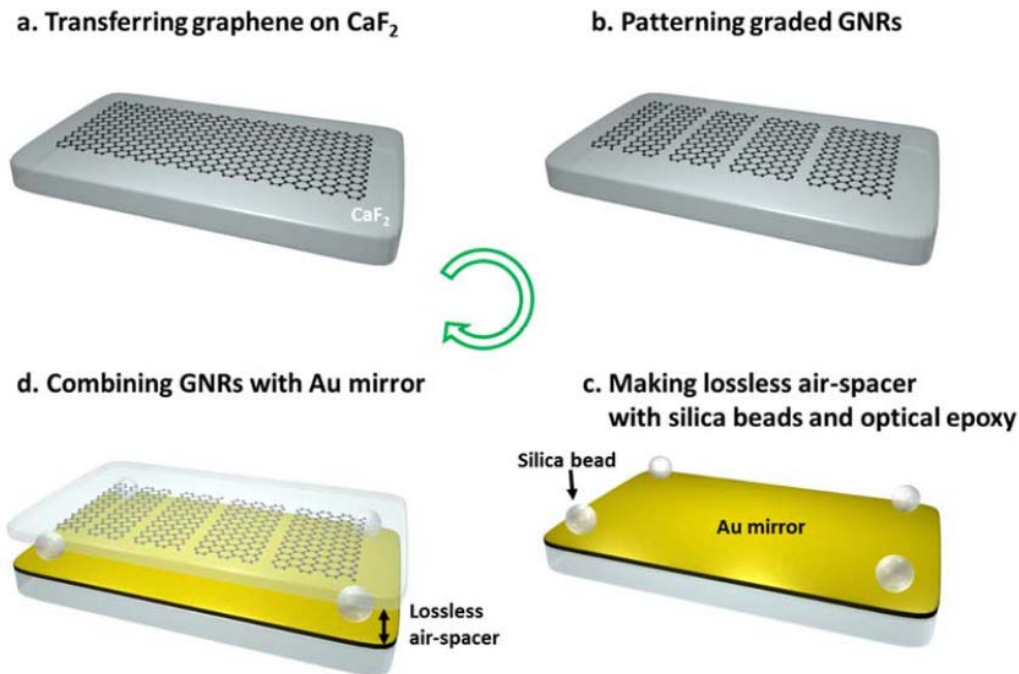


Figure 2. Fabrication schematics of graded graphene nano-ribbon reflectarray with lossless air-spacers.

The image of the GNR reflectarray fully integrated with the Au mirror and an air-spacer is shown in Figure 3a. GNR patterns on CaF₂ are hard to locate, so to aid in the sample alignment we add alignment marks and record the map images prior to the PMMA removal to locate the GNR patterns (Figure 3b). The GNR pattern includes five supercells with 40 μm by 200 μm (Figure 3c). The fully assembled GNR reflectarray will be operated in an internal reflection configuration as illustrated in Figure 3d.

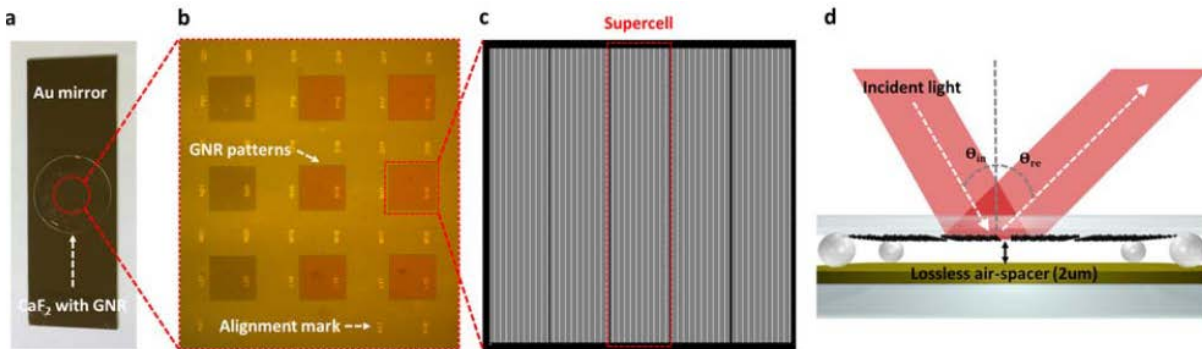


Figure 3. Images of a GNR reflectarray. (a) Photograph of a GNR reflectarray chip. (b) Zoomed-in image of GNR reflectarray with alignment marks. The size of GNR patterns is 200 μm by 200 μm . (c) CAD image of GNR pattern including five supercells.

The size of supercell is 40 μm by 200 μm . Five supercells are placed side by side and the entire size of GNR reflectarray is 200 μm by 200 μm . (d) Illustration of a side-view image of GNR reflectarray.

The supercell was patterned on the CaF₂ substrate using PMMA and electron beam lithography. The fabricated supercell is a series of 200 graphene ribbons with widths varying from 50 nm to 150 and 200 nm period shown in Figure 4, which results in an operating wavelength of 11 μm .

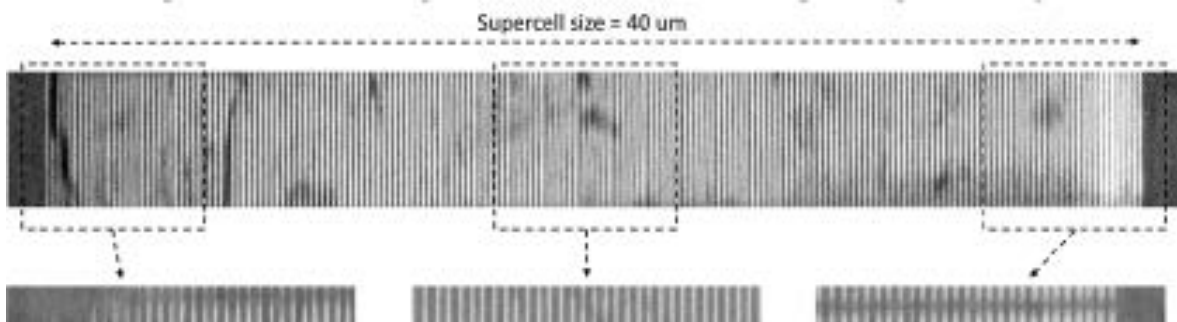


Figure 4. SEM images of a supercell of GNR reflectarray on CaF₂. The horizontal length of a supercell including 200 GNRs is 40 μm .

Modeling of GNR reflectarray

Anomalous reflection is achieved with an array of graphene nanoribbons with varying widths. The widths are chosen such that they impart a constant scattering phase gradient along the plane of incidence [1]. The amount of scattering phase imparted by the graphene nanoribbon can be estimated analytically or computed numerically [2]. This allows us to design a graphene reflectarray device where the widths are chosen so it imparts a constant scattering phase gradient along the plane of incidence, and therefore obtain an anomalous reflection angle that differs from the traditional angle of specular reflectance.

We simulate a single supercell of the full reflectarray device with COMSOL Multiphysics. Figure 5 shows the scattered field for normal (Fig. 5a) and 10 degree (Fig. 5b) incident plane waves. The simulation assumes parameters corresponding to the experimental conditions; a typical electron relaxation time of $\tau=0.6$ ps [4], a refractive index of 1.27 for the underlying CaF₂ substrate, incident light at wavelength of 11 μm , and graphene doping at a Fermi level of 0.3 eV. With these parameters, simulations reveal a beam steering angle that differs from the specular reflection beam by approximately 12 degrees. We emphasize that in these simulations, the CaF₂ substrate is assumed to be lossless. Indeed, CaF₂ is often a substrate of choice in the mid-infrared since it does not have prominent infrared active phonons in this regime. Hence, finite losses in the dielectric should still be expected.

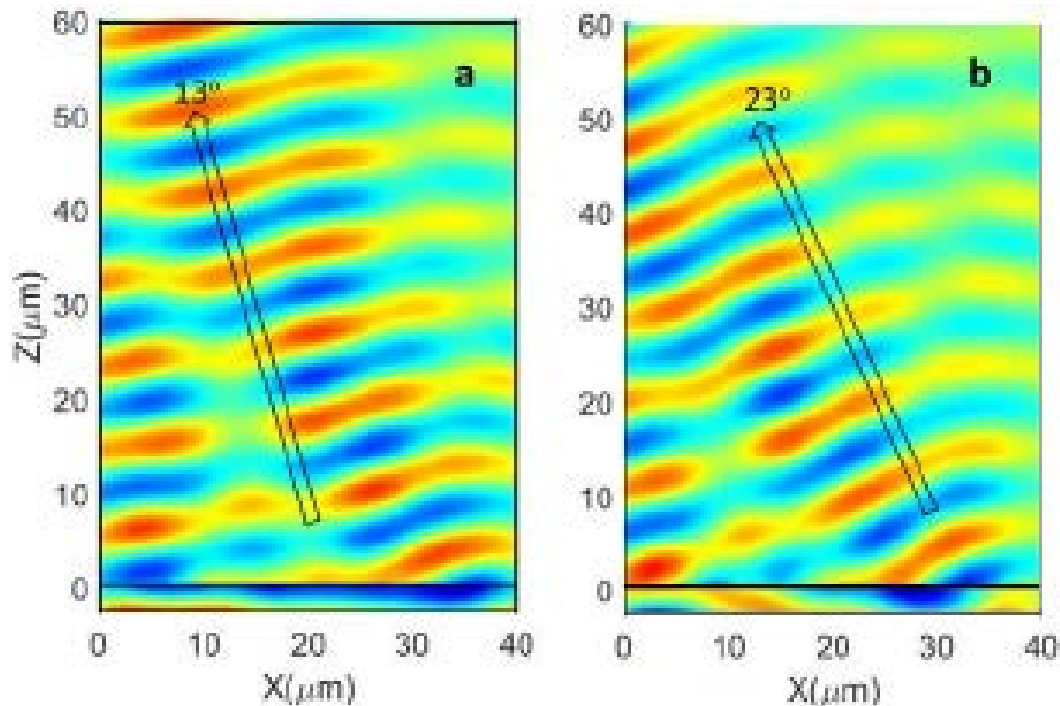


Figure 5. Reflected field off the graphene reflectarray device for (a) normal and (b) oblique (10 degrees off normal) incident light.

The device is designed to produce an anomalous reflection of 12 degrees at a doping level of 0.3eV. Figure 6 shows normal-incidence, far-field plots for different GNR doping levels. As shown, away from 0.3eV, the intensity of the anomalous reflection is reduced and specular reflection is recovered. The strong dependence of the anomalous reflection intensity with doping can allow us to distinguish between anomalous and specular beams in the experiments. Here, we also note that the device utilizes a metallic back mirror separated by a quarter wavelength distance from the graphene ribbon array, which serves to maximize the interaction with the graphene ribbon array [2].

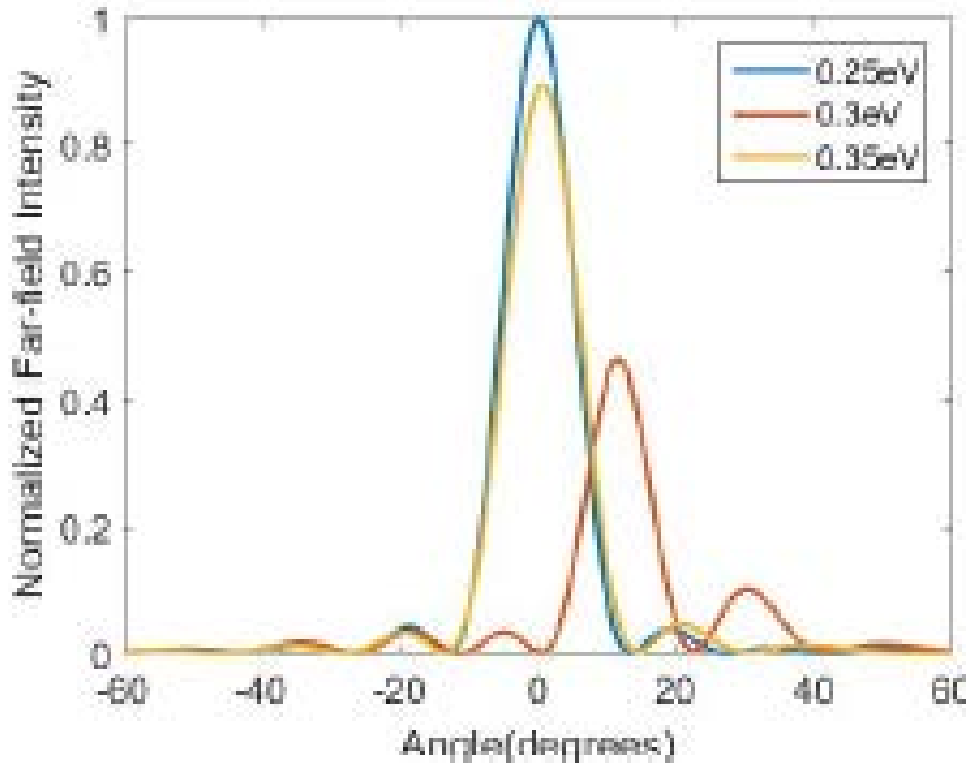


Figure 6. Normalized far-field intensity as function of angle for different dopings for normal incident light. Specular beams are at zero degrees.

Finally, we discuss the impact of dielectric loss on the performance of the device. First, our simulation shows that the intensity of the anomalous beam will diminish relative to the specular beam. Secondly, the anomalous angle will also decrease as the dielectric losses increase.

The availability of 2π phase shift of the structure with optical cavity is dependent on the intrinsic losses in the system. The losses can originate from either graphene or the substrate. Figure 7a shows the phase profile for a unit cell of the device with increasing substrate losses (imaginary refractive index, k). As we can see, beyond a certain value ($k=0.01$) we do not have the 2π phase shift.

Similar behavior can be seen when the relaxation time of graphene is reduced. This can be explained by coupled mode theory for a single resonator with external excitation. The reflection coefficient for this can be calculated as:

$$r = \frac{\gamma_r - \gamma_a - i(\omega - \omega_0)}{\gamma_r + \gamma_a + i(\omega - \omega_0)}$$

$\gamma_r \sim$ radiative losses, $\gamma_a \sim$ absorptive/intrinsic losses. This is plotted in complex plane in Figure 7b. When intrinsic losses are high, the circles do not cover all four quadrants anymore which results in losing the phase range of 2π . We believe that our current device structure, where the graphene ribbons are suspended, see Fig. 3c, has allowed us to alleviate a large part of this problem due to substrate loss. However, losses from the graphene plasmons itself might still persists, which is an issue we have to address at next stage of the program.

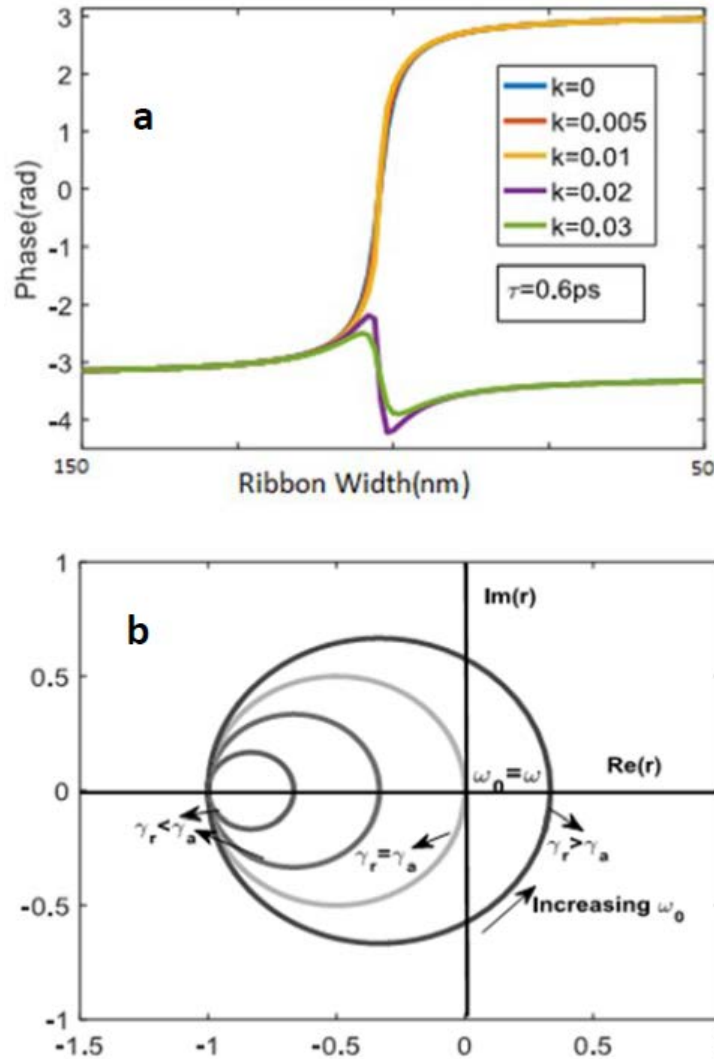


Figure 7. (a) Impact of dielectric loss on scattering phase. (b) Complex plane plot of the reflection coefficient for analytical model of the structure as a single port resonator

Scatterometry measurement

We have built a scatterometer that is capable of imaging the angular resolved optical scattering of microscale nanostructures. A schematic of this instrument is shown in Figure 8. The light source consists of a tunable quantum cascade laser that operates in the range of $\lambda = 6 - 12 \mu\text{m}$. A series of mirrors are used to steer the incident beam through a ZnSe objective with a clear aperture of 5mm and working distance of 17.5 mm, which focuses the beam onto the sample with a beam diameter of approximately $100 \mu\text{m}$. The total angular spread of the incident beam is approximately 4° . The sample is mounted on a rotation stage that is used to vary the angle of incidence (θ_i), which is the angle between the incoming light and normal to the sample. A ZnSe collection objective (same specifications as the focusing objective) and liquid-nitrogen-cooled HgCdTe detector are mounted to a second rotation stage and rotate together as a single unit. Scattered light that impinges upon the objective is focused onto the detector and the detector signal is recorded by the computer. By revolving the collection objective and detector around the sample, the angle dependent scattering profile of the sample can be mapped. It should be noted that for this initial experiment the incident light polarization is oriented 45° from the width of the ribbons. The scattering profile of the graphene nanoribbon reflectarrays (GNR) is measured for $\lambda = 11 \mu\text{m}$, and a detection angles in the range of $\theta_d = 25 - 60^\circ$ (this is the angle between normal to the sample surface and the detector see Figure 2).

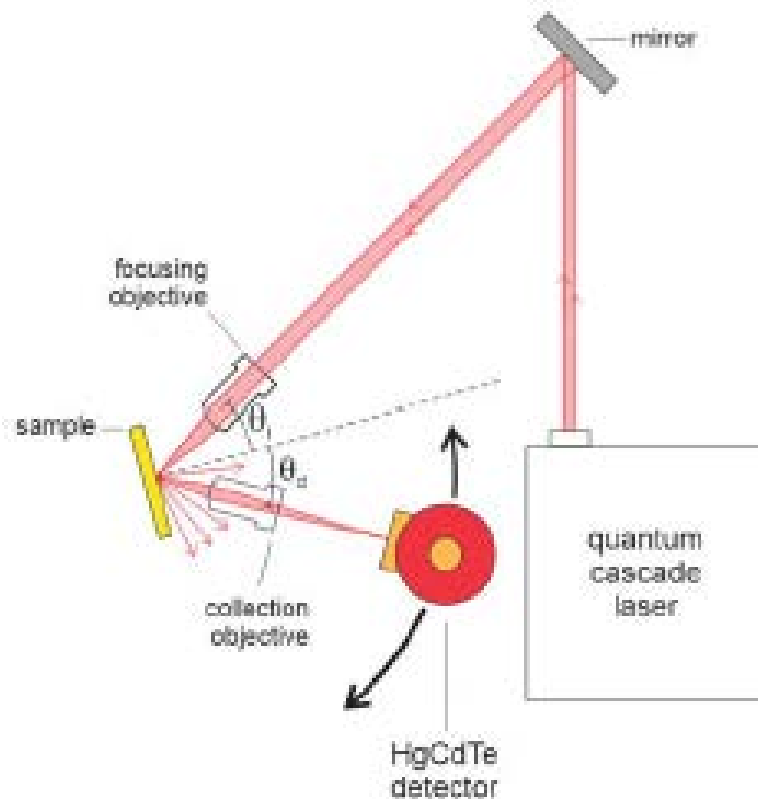


Figure 8. Schematic of the scatterometer setup.

Prior to mounting the sample in the scatterometer, the GNR reflectarray graphene was chemically doped using nitric acid vapor. This is achieved by filling a 500 ml beaker with 100 ml of Nitric acid (69%), the graphene sample was then placed on top of the beaker, with the GNR reflectarrays facing the nitric acid. A 1000 ml beaker is then placed upside down over the system (see Figure 9). The system is left in this doping configuration for 20 minutes. To confirm doping of the reflectarray, polarized reflectance spectra of uniform GNR was measured in an FTIR microscope immediately after doping (see Figure 9a-b for plots of R_{per} , R_{par} , and $1-R_{per}/R_{par}$).

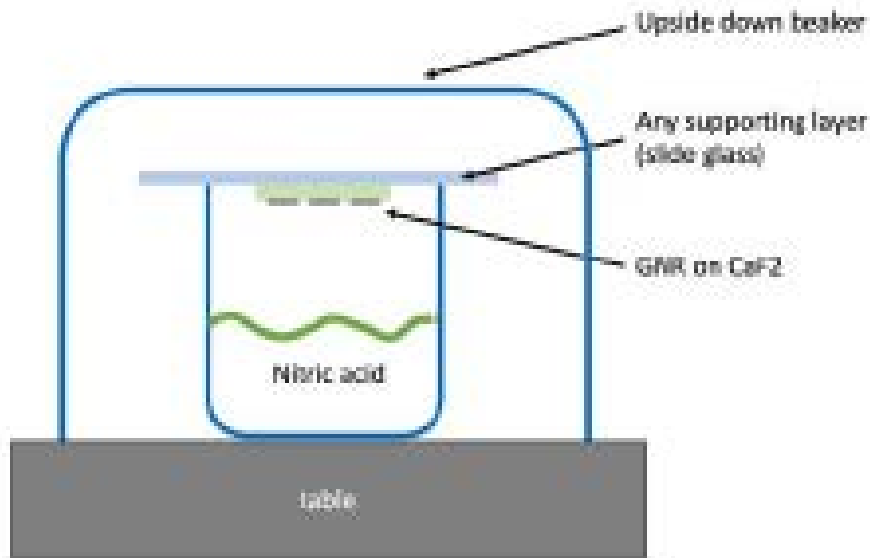


Figure 9. Schematic of the doping configuration.

After measuring the reflectance of the uniform GNRs, the sample was mounted in the scatterometer and the system was aligned. Unfortunately, we have no way to image the sample once it is mounted in the scatterometer, so aligning the QCL onto the $200 \times 200 \mu m$ GNR reflectarrays patterns is challenging. However, we are able to align the system using a masking technique that has been successful in prior experiments where the sample cannot be imaged [3]. The masking technique involves placing two pieces of doubled sided sticky tape near the GNR patterns. The two pieces of tape that are orthogonally oriented serve as a coordinate system for locating the GNR reflectarrays, where the intersection of the two pieces of tape serves as the origin. Prior to mounting the sample in the scatterometer, we use an optical microscope to image the tape and GNR reflectarray patterns. This allows us to determine the position of the GNR reflectarray patterns with respect to the tape coordinate system. The sample is then mounted in the scatterometer. The tape is a poor reflector of infrared light, therefore, by scanning the laser position across the sample and looking for a sharp decrease in the reflectance, we can determine the position and orientation of the tape when the sample is mounted in the scatterometer. Once we have the position and orientation of the tape coordinate system, we can then reposition the sample so that the laser is incident upon the GNR pattern.

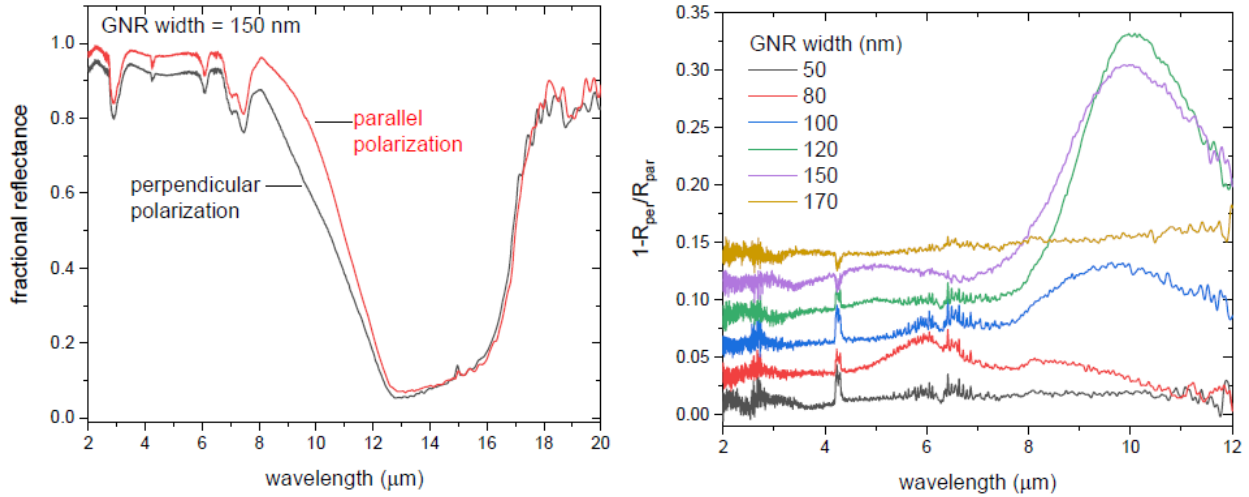


Figure 10. (a) Fractional polarized reflectance of uniform GNR pattern with width of 150 nm, where light is polarized parallel (red) and perpendicular to the GNRs. (b) Extinction spectra for GNR pattern of varying ribbons width.

Figure 11 summarizes the results of normalized scatterometry measurements that are collected over a period of 61.5 hours, where the angle of incidence is fixed at 30° and the detector position is swept over the range $\theta_{det} = 25 - 60^\circ$ (as defined in Figure 1). Here we present the normalized data since over time the power of the QCL fluctuated with time. In general, five peaks are detected in the angle dependent scattering that are centered around $\theta_{det} = 15, 17.3, 19.6, 23.4$ and 27.4° (labeled by numerals 1-5 in the top panel of Figure 10). The origins of each peak are not fully understood at the moment; however, these results clearly show that the intensity of peaks 2- 5 change as time increases and the doping level decreases. In general, the relative intensity of most observed peaks monotonically increase (peaks 3 and 5) or decrease (peak 4) with time. However, peak 2 shows non-monotonic behavior that may be associated with hitting a sweet-spot doping level that maximizes the intensity of a reflection that has been steered due to tailoring the phase of GNR plasmon resonances. Initially, at time $t = 0$ hours peak 2 exists as a weak shoulder that appears near $\theta_{det} = 32.3^\circ$ (top panel of Figure 10). As time increases, as shown in the middle panel of Figure 10 at $t = 24.65$ hours, the relative strength of peak 2 increases to the point where this peak can be easily distinguished from peak 1. This may correspond to the point where the GNR is optimally doped at which point a maximum proportion of the reflected light is diverted to the steered beam. As time increases further, as shown in the third panel of Figure 11 at $t = 61.45$ hours, the relative intensity of peak 2 decreases back to the point where it is a shoulder on peak 1, which may correspond to the point where the graphene doping level is less than the optimum value and less light is diverted to the steered beam.

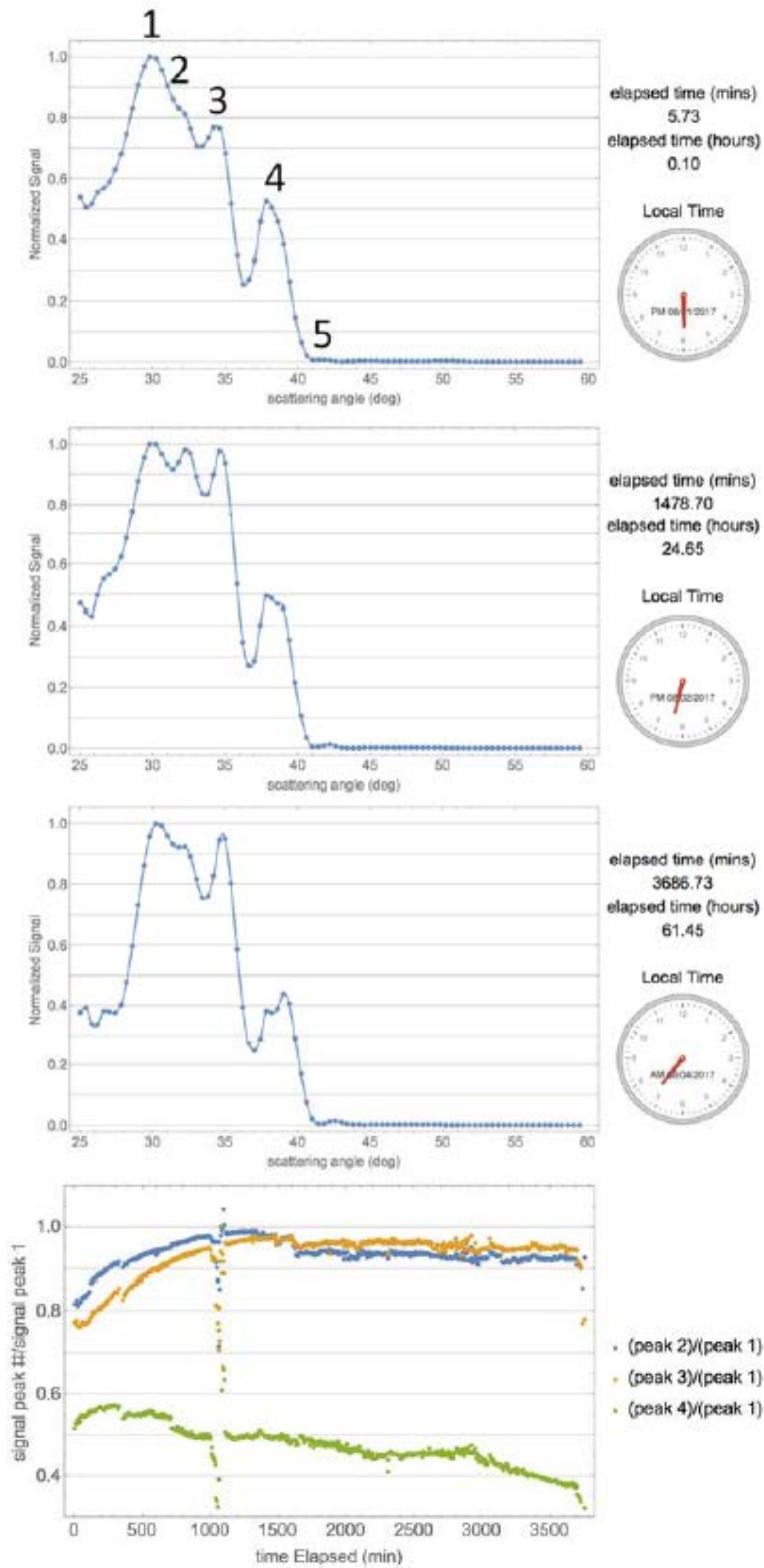


Figure 11. Normalized scattering intensity as a function of detector angle, and relative intensity of scattering peaks normalized to intensity of peak 1.

Exploring broader device applications

On the modeling front, we continue our exploration of new application space of our graphene reflectarray. In Figure 12, we illustrate some of the possible applications. Figure 12b shows that one can implement the metasurface to an arbitrary surface and tailor the local phase so that the scattered reflected light would mimic that from a flat surface, i.e. cloaking. A simple extension of this idea would also mean that we can produce reflected light that mimics scattering of different surfaces shown in Figure 12c, i.e. illusion optics. In addition, we can also incorporate anomalous reflections in conjunction with cloaking or illusion optics as illustrated in Figure 12d. Lastly, one can also achieve reflective focusing of far-field to a near-field focal point.

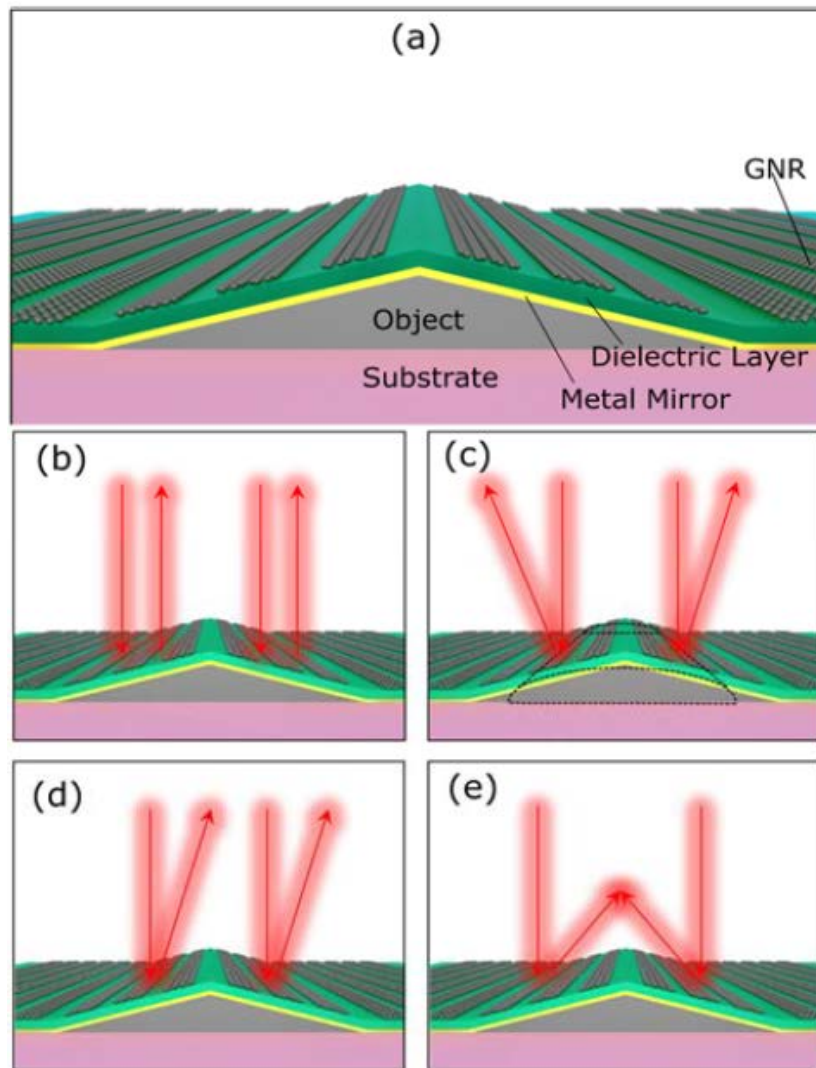


Figure 12. Schematics showing how one can utilize the graphene based reflectarray for various functionalities such as (b) cloaking, (c) illusion, (d) anomalous reflection, and (e) focusing.

In all these implementations, we used arrays of graphene ribbons with equal width but different dopings for each ribbon according to the desired phase profile. Hence, the device is tunable and

can achieve all these operations within the same metasurface. In particular, we show the simulation result for reflective focusing off an arbitrary surface in Figure 13. Figure 13a-c shows the field intensity plots for focusing of an incident plane wave to a focal distance of $150\mu\text{m}$ from the ground plane. Figure 13 a-b show normal incidence while Figure 13c shows result for a 30 degree incidence. In Figure 13a and c, the focal point is located $150\mu\text{m}$ away in the normal direction while in Figure 13b the focal point is at an angle of 30 degrees. Figure 13d shows focusing of a point dipole source.

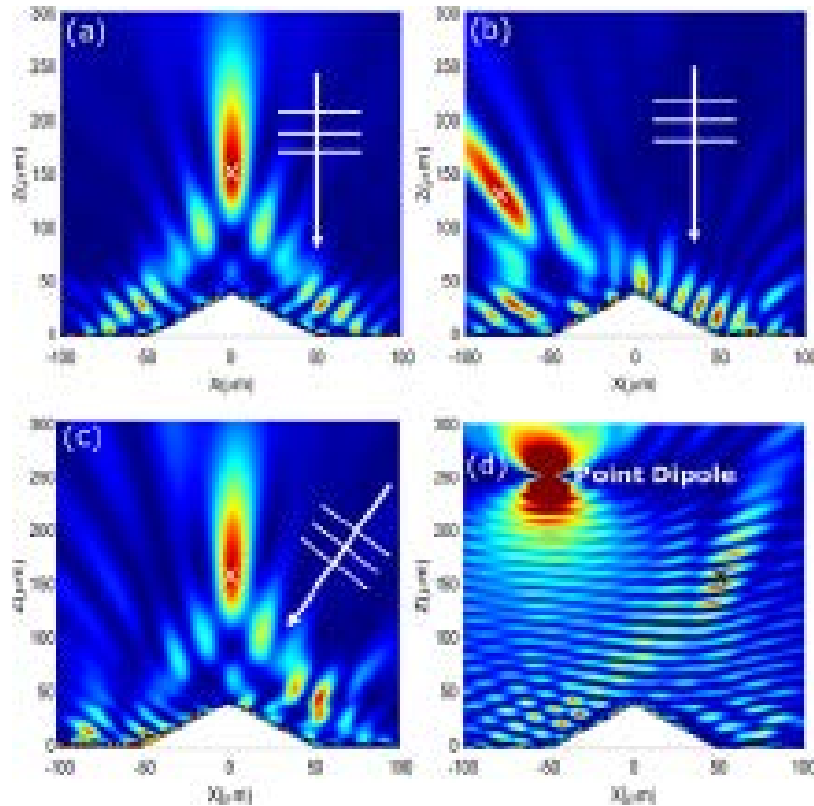


Figure 13. Simulation results for reflective focusing off arbitrary surface.

These results are currently being summarized in a manuscript to be submitted for publication.

Future Plans

We summarized the key lessons and achievements in this seedling program:

- We have successfully developed the fabrication process for “substrate free” graphene reflectarray where full 2π phase is in principle achievable.
- Scatterometry measurement of the anomalous phase of graphene reflectarray was established and demonstrated.
- Strong signatures of anomalous beam, an angular resolved beam that is optimal at particular doping, was identified in the measurement. Hence, the seedling conclude the proof-of-principle demonstration. Nitric acid was used in the seedling phase as doping scheme and its evaporation with time allows us to vary the doping.
- Device design protocols are in place for subsequent optimization of the graphene reflectarray device in the next step.
- Several technical issues are identified and has to be overcome in the next step, which we elaborate below.

The following immediate next steps are proposed:

- Our current beam spot size is $200\ \mu\text{m} \times 200\ \mu\text{m}$, and there is still room for focusing this down with a newly acquired set of optical lenses. It will be advantageous to reduce the beam spot size further so the device can be scaled down and phase gradient can be increased.
- Polarization dependent scatterometry measurement should be performed in order to isolate effects from graphene plasmons versus that due to ordinary scattering effects
- Scatterometry with in-situ camera system will be setup in the next phase, and this will ensure better device alignment in the measurement.
- Since we have identified design parameters, we are ready to produce larger-area reflectarray device as ideally the device should be larger than the beam spot size. This is certainly achievable in the next step. A small device was used in the seedling stage as we determined this to be sufficient for proof-of-principle demonstration.
- Electrical gating will be implemented in the next phase. Prior work by IBM [5] has already demonstrate electrical tuning of plasmon resonance with 100nm SiO₂ substrate with tunability of about 10cm^{-1} for every 5V. Our device will have 50 times less capacitance, hence this will require voltage of order 100V in order to sufficiently tune the plasmon resonance. High voltage sources are available at NRL for our testing.
- Systematic understanding of the origin of the multiple peaks will be performed, and we will incorporate this mechanism to model the actual device.
- We will design, optimize and demonstrate a reflectarray with anomalous beam of $>50\%$ of the incident power, an anomalous angle of 10° , and ultrafast beam steering in timescale of micro-seconds (orders faster than conventional micro-mirrors).

References

1. Yu N, Genevet P, Kats MA, Aieta F, Tetienne JP, Capasso F, Gaburro Z. Light propagation with phase discontinuities: generalized laws of reflection and refraction. *science*. 2011 Oct 21;334(6054):333-7.
2. Carrasco E, Tamagnone M, Mosig JR, Low T, Perruisseau-Carrier J. Gate-controlled mid-infrared light bending with aperiodic graphene nanoribbons array. *Nanotechnology*. 2015 Mar 11;26(13):134002.
3. Nolde JA, Kim M, Kim CS, Jackson EM, Ellis CT, Abell J, Glembocki OJ, Canedy CL, Tischler JG, Vurgaftman I, Meyer JR. Resonant quantum efficiency enhancement of midwave infrared nBn photodetectors using one-dimensional plasmonic gratings. *Applied Physics Letters*. 2015 Jun 29;106(26):261109.
4. Yan H, Low T, Zhu W, Wu Y, Freitag M, Li X, Guinea F, Avouris P, Xia F. Damping pathways of mid-infrared plasmons in graphene nanostructures. *Nature Photonics*. 2013 May 1;7(5):394-9.
5. Freitag M, Low T, Zhu W, Yan H, Xia F, Avouris P. Photocurrent in graphene harnessed by tunable intrinsic plasmons. *arXiv preprint arXiv:1306.0593*. 2013 Jun 3.

LIST OF SYMBOLS, ABBREVIATIONS, AND ACRONYMS

AFRL	Air Force Research Laboratory
DARPA	Defense Advanced Research Project Agency
DTIC	Defense Technical Information Center
FTIR	Fourier Transform Infrared Spectroscopy
GNR	Graphene nano-ribbon
NRL	Navy Research Laboratory
RXAN	Nanoelectronic Materials Branch, Functional Materials Division, Materials and Manufacturing Directorate